JPET Fast Forward. Published on March 26, 2020 as DOI: 10.1124/jpet.119.264499
This article has not been copyedited and formatted. The final version may differ from this version.

JPET # 264499

Pharmacokinetic-Pharmacodynamic-Efficacy Modeling of ONO-7579, a Novel Pan-TRK Inhibitor, in a Murine Xenograft Tumor Model

Hiroyuki Iida, Ryu Fujikawa, Ryohei Kozaki, Ryuichi Harada, Yuya Hosokawa, Ken-ichi Ogawara, Tomoya Ohno

Clinical Pharmacology (H.I., T.O.), Research Center of Oncology (R.F., R.K.), and Pharmacokinetic Research Laboratories (R.H., Y.H.), Ono Pharmaceutical Company Limited, Osaka, Japan; and Laboratory of Pharmaceutics, Kobe Pharmaceutical University, Higashinada-ku, Kobe, Japan (H.I., K.O.)

Downloaded from jpet.aspetjournals.org at ASPET Journals on April 20, 2024

JPET Fast Forward. Published on March 26, 2020 as DOI: 10.1124/jpet.119.264499
This article has not been copyedited and formatted. The final version may differ from this version.

JPET # 264499

Running Title:

PK/PD/Efficacy Modeling of a TRK Inhibitor in Mice

Corresponding author:

Hiroyuki Iida

Clinical Pharmacology

Ono Pharmaceutical Co., Ltd.

3-1-1 Sakurai, Shimamoto-cho, Mishima-gun, Osaka 618-8585, Japan

Phone: +81 75 961 1166

Fax: +81 75 961 1182

E-mail: hi.iida@ono.co.jp

Number of text pages: 41

Number of tables: 5

Number of figures: 6

Number of references: 30

Number of words in the Abstract: 246

Number of words in the Introduction: 421

Number of words in the Discussion: 1225

Downloaded from jpet.aspetjournals.org at ASPET Journals on April 20, 2024

JPET Fast Forward. Published on March 26, 2020 as DOI: 10.1124/jpet.119.264499
This article has not been copyedited and formatted. The final version may differ from this version.

List of nonstandard abbreviations:

ECL, electrochemiluminescence;

LC/MS/MS, liquid chromatography/tandem mass spectrometry;

MTD, maximum tolerated dose;

NTRK, neurotrophic tyrosine receptor kinase;

OFV, objective function value;

ONO-7579, N-{2-[4-(2-amino-5-chloropyridin-3-yl)phenoxy]pyrimidin-5-yl}-N'-[2-(methanesulfonyl)-5-(trifluoromethyl)phenyl]urea;

PD, pharmacodynamic;

PK, pharmacokinetic;

pTRKA, phosphorylated TPM3-TRKA

TRK, tropomyosin receptor kinase;

Recommended Section Assignment:

Drug Discovery and Translational Medicine

Downloaded from jpet.aspetjournals.org at ASPET Journals on April 20, 2024

JPET Fast Forward. Published on March 26, 2020 as DOI: 10.1124/jpet.119.264499
This article has not been copyedited and formatted. The final version may differ from this version.

Abstract

An orally available and novel small molecule, ONO-7579 (N-{2-[4-(2-amino-5-chloropyridin-3-yl)phenoxy]pyrimidin-5-yl}-N'-[2-(methanesulfonyl)-5-(trifluoromethyl)phenyl]urea), is a highly potent and selective pan-tropomyosin receptor kinase (TRK) inhibitor. The objective of the present study was to characterize the pharmacokinetic (PK), pharmacodynamic (PD), and antitumor efficacy relationships of ONO-7579 in mice xenografted with a human colorectal cancer cell line, KM12 (harboring the *TPM3-NTRK1* fusion gene), via a PK/PD modeling approach. Plasma and tumor concentrations of ONO-7579, tumor levels of phosphorylated TPM3-TRKA (pTRKA), and tumor volumes in the murine model were measured with a single or multiple dose of ONO-7579 0.06–0.60 mg/kg administered once daily. The PK/PD/efficacy models were developed in a sequential manner. Changes in plasma concentrations of ONO-7579 were described with an oral one-compartment model. Tumor concentrations of ONO-7579 were higher than plasma concentrations, and changes in ONO-7579 tumor concentrations were described with an additional tumor compartment that had no influence on plasma concentrations. pTRKA in tumors was described with a direct E_{max} model, and the tumor ONO-7579 concentration causing 50% of the maximum effect was estimated to be 17.6 ng/g. In addition, a pTRKA-driven tumor growth inhibition model indicated that ONO-7579 started to sharply increase the antitumor effect at pTRKA inhibition rates >60%, and required >91.5% to reduce tumors. In conclusion, the developed PK/PD/efficacy models revealed a "switch-like" relationship between pTRKA inhibition rate and antitumor effect in a murine KM12 xenograft model, demonstrating that pTRKA in tumors could serve as an effective biomarker for scheduling the dose regimen in early-stage clinical studies.

Downloaded from jpet.aspetjournals.org at ASPET Journals on April 20, 2024

JPET Fast Forward. Published on March 26, 2020 as DOI: 10.1124/jpet.119.264499
This article has not been copyedited and formatted. The final version may differ from this version.

Significance Statement

In recent years, clinical development of TRK inhibitors in patients with *NTRK* fusion-positive solid tumors has been accelerated. This research found that phosphorylated TRKA was a useful biomarker for explaining the antitumor efficacy of TRK inhibitors using a PK/PD modeling approach in xenograft mice. This finding suggests a rational dosing regimen in early-stage clinical studies for ONO-7579, a novel pan-TRK inhibitor.

Downloaded from jpet.aspetjournals.org at ASPET Journals on April 20, 2024

JPET Fast Forward. Published on March 26, 2020 as DOI: 10.1124/jpet.119.264499
This article has not been copyedited and formatted. The final version may differ from this version.

Introduction

Neurotrophic tyrosine receptor kinase (*NTRK*) *1*, *NTRK2*, and *NTRK3* genes encode tropomyosin receptor kinase (TRK) A, TRKB, and TRKC, respectively, which are members of the TRK family of receptor tyrosine kinases (Friedman et al., 2015). TRKA, TRKB, and TRKC play an important role in both central and peripheral nervous systems, regulating cellular proliferation, synaptic plasticity, neurite outgrowth, neuron maintenance, and apoptosis (Deinhardt and Chao, 2014). Recently, oncogenic rearrangements of *NTRK1*, *NTRK2*, and *NTRK3* genes were identified in various cancers, and several fusion partners between 5-prime and 3-prime *NTRK* genes have been reported (Lange and Lo, 2018). These oncogenic rearrangements of *NTRK* encode chimeric proteins with constitutive kinase activity, which promote tumor cell growth and survival.

Entrectinib and larotrectinib are being developed as pan-TRK inhibitors, and results from clinical studies of these compounds indicate that both drugs are well tolerated with dramatic clinical efficacy responses in cancer patients harboring *NTRK* rearrangement (Drilon et al., 2018; Laetsch et al., 2018; Drilon et al., 2017b). Meanwhile, LOXO-195 is being developed as a second-generation TRK inhibitor, which will overcome challenges of drug resistance to first-generation TRK inhibitors (Drilon et al., 2017a).

ONO-7579 (N-{2-[4-(2-amino-5-chloropyridin-3-yl)phenoxy]pyrimidin-5-yl}-N'-[2-(methanesulfonyl)-5-(trifluoromethyl)phenyl]urea), expected to be a second-generation pan-TRK inhibitor, is a highly potent and selective oral pan-TRK inhibitor that selectively inhibits TRK autophosphorylation associated with downstream signaling (Kawamoto et al., 2018).

Preclinical translational pharmacokinetic (PK)/pharmacodynamic (PD) modeling has facilitated drug development (Wong et al., 2017). Determination of recommended doses in

Downloaded from jpet.aspetjournals.org at ASPET Journals on April 20, 2024

JPET Fast Forward. Published on March 26, 2020 as DOI: 10.1124/jpet.119.264499
This article has not been copyedited and formatted. The final version may differ from this version.

recent early-stage oncologic clinical development of molecularly-targeted agents has been shifting from traditional maximum tolerated dose-based strategies to finding biologically effective dose-based strategies using effect markers (Sachs et al., 2016). In preclinical research with kinase inhibitors, a relationship between kinase phosphorylation and antitumor efficacy in xenograft mice was analyzed using a PK/PD model, and a clinical dose based on a PD biomarker was discussed in a prospective or retrospective manner (Yamazaki et al., 2015; Yamazaki, 2013; Wong et al., 2012; Wang et al., 2009). To the best of our knowledge, the *in vivo* PK/PD characterization of a drug acting on the TRK pathway, based on a modeling approach, has not yet been described.

In this article, phosphorylated TPM3-TRKA (pTRKA) is assessed for its effectiveness as a biomarker. The relationship between pTRKA in tumors and antitumor efficacy after ONO-7579 administration is analyzed using a PK/PD modeling approach in mice xenografted with a human colorectal cancer cell line, KM12 (harboring the *TPM3-NTRK1* fusion gene) (Doebele et al., 2015). This PK/PD modeling approach was implemented to enable determination of the appropriate dosing regimen for early-stage clinical development.

Downloaded from jpet.aspetjournals.org at ASPET Journals on April 20, 2024

JPET Fast Forward. Published on March 26, 2020 as DOI: 10.1124/jpet.119.264499
This article has not been copyedited and formatted. The final version may differ from this version.

Materials and Methods

Compound

ONO-7579 (purity ≥95%) was synthesized by Medicinal Chemistry Research Laboratories, Ono Pharmaceutical Co., Ltd (Osaka, Japan); the chemical structure is shown in Figure 1. ONO-7579 was orally administered to mice as a solution containing 20% v/v solvent: Kolliphor HS 15 (BASF Japan, Tokyo, Japan) and propylene glycol (Maruishi Pharmaceutical, Osaka, Japan) were mixed at volume ratio of 7:3, with two equivalent amounts of methanesulfonic acid.

Animal studies

A suspension of KM12 cells (American Type Culture Collection, Manassas, VA, USA) was injected subcutaneously (0.1 mL, 5×10^7 cells/mL) into 6-week-old female BALBnu/CrlCrlj mice (Charles River Laboratories Japan, Kanagawa, Japan). When the mean tumor volume reached 80–200 mm^3, the mice were randomized into treatment groups according to their individual tumor volumes. The mice were then used in a single-dose PK/PD study and a multiple-dose tumor growth study. All studies were conducted in accordance with "Efficacy Pharmacology at Research Headquarters: Standards for Reliance," established by Ono Pharmaceutical Co., Ltd. All studies also complied with "Guidance for Animal Experiments," and safety procedures (e.g., procedures dealing with pathogens), all of which were established by Ono Pharmaceutical Co., Ltd.

PK/PD study (single administration). The mice were assigned to groups 9 days after KM12 was transplanted. A single oral administration of ONO-7579, at doses of 0.06 and 0.60 mg/kg, was given 2 days after the day of assignment. Nothing was administered to the mice assigned to

Downloaded from jpet.aspetjournals.org at ASPET Journals on April 20, 2024

JPET Fast Forward. Published on March 26, 2020 as DOI: 10.1124/jpet.119.264499
This article has not been copyedited and formatted. The final version may differ from this version.

the control group. Blood samples were collected from mice in the control group and from mice in the ONO-7579 groups, at 2, 4, 7, 24, 38, and 48 h after ONO-7579 administration (n=4/time point; blood samples 38 and 48 h after administration were collected only from the ONO-7579 0.60 mg/kg group). Besides the xenograft mice, normal mice (no transplantation) were given a single dose of ONO-7579 (0.1, 0.3, 1.0 mg/kg; 1, 2, 4, 8, 24 h; n=3/time point) to enrich absorption-phase PK data. The collected blood samples were centrifuged at 13,400 *g* for 3 min at 4°C, and the supernatant was collected as plasma. The plasma was cryopreserved at −80°C and used for measurement of plasma ONO-7579 concentrations. The mice were exsanguinated after blood collection and tumors in the back of the neck were collected. The collected tumors were cleansed with saline and were then cut into two pieces. The tumor pieces were cryopreserved at −80°C and used for measurement of tumor ONO-7579 concentrations and pTRKA in tumors.

Tumor growth study (multiple administration). The mice were assigned to groups 3 days after KM12 was transplanted. Vehicle or ONO-7579 was orally administered once daily for 12 days at 0.06, 0.20, or 0.60 mg/kg (n=8/group), starting on the day of assignment. The long and short axes of tumors were measured using electronic calipers (Mitutoyo Corporation, Kanagawa, Japan) every 2 or 3 days after treatment initiation, and tumor volume was calculated using the formula (volume = width^2 × length × 0.5). ONO-7579 was orally administered on day 13 to examine PK/PD at the time of multiple administration. Blood samples and tumor samples were collected 4 and 24 h after administration (n=4/time point). The collected samples were handled in the same manner as in the PK/PD study.

Downloaded from jpet.aspetjournals.org at ASPET Journals on April 20, 2024

JPET Fast Forward. Published on March 26, 2020 as DOI: 10.1124/jpet.119.264499
This article has not been copyedited and formatted. The final version may differ from this version.

Assay

ONO-7579. ONO-7579 in plasma was extracted by a solid-phase extraction method using Oasis PRiME HLB μElution Plate (Waters, Milford, MA, USA). Tumor samples were homogenized in distilled water, and ONO-7579 was extracted with acetonitrile/ethanol (7:3, v/v). Plasma and tumor ONO-7579 concentrations were determined by liquid chromatography/tandem mass spectrometry (LC/MS/MS). The LC/MS/MS system consisted of the Shimadzu Nexera MP system (Shimadzu Corporation, Kyoto, Japan) and an API 4000 triple-stage quadrupole mass spectrometer (Applied Biosystems, Foster City, CA, USA). Both instruments were controlled by Analyst 1.6.2 software (Applied Biosystems). Chromatographic separation of the analytes was achieved using a reverse phase column (InertSustain C18, 2.1 mm × 50 mm, 3 μm; GL Sciences, Tokyo, Japan) at a flow rate of 0.5 mL/min. A binary mobile phase consisted of water with 10 mmol/L ammonium formate (A) and methanol (B). The gradient started at 75% B for 2 min, increased to 90% B over 0.1 min, and then held at 90% B for 0.9 min. The gradient was returned to the initial condition of 75% B in 0.1 min and equilibrated at 75% B for 1.9 min before the next injection. The total cycle time for one injection was 5 min. The mass spectrometer was operated in the negative ionization mode using multiple reaction monitoring at a specific precursor ion → product ion transition: m/z 576.9 → 237.8.

pTRKA. The amount of pTRKA in tumors was measured with an electrochemiluminescence (ECL) method according to the Meso Scale Discovery (Rockville, MD, USA) manufacturer's protocol. Briefly, cryopreserved tumors were pulverized in cell lysis buffer by multi-beads shocker. The pulverized tumors in cell lysis buffer were thereafter centrifuged, and the supernatant was collected as tumor lysate. Tumor lysate was diluted with cell lysis buffer and

Downloaded from jpet.aspetjournals.org at ASPET Journals on April 20, 2024

JPET Fast Forward. Published on March 26, 2020 as DOI: 10.1124/jpet.119.264499
This article has not been copyedited and formatted. The final version may differ from this version.

used as a sample in the ECL method. Plate coating and sandwich immunoassay in the ECL method were conducted with the antibodies shown in Table 1 and as described in the protocol provided with the MULTI-ARRAY 96-well Plate (Meso Scale Discovery). The amounts of pTRKA and total TRKA were measured as intensity of light with a plate reader (MESO QuickPlex SQ 120; Meso Scale Discovery). The amount of pTRKA was normalized with the amount of total TRKA and used for analysis.

Data analysis

All model analyses were performed with NONMEM 7.1.2 (ICON Development Solutions, Ellicott City, MD, USA). Figure 2 shows a graphical abstract of the PK/PD/efficacy models. The PK/PD/efficacy models were developed sequentially (with model parameters fixed) in an order of: PK model describing plasma concentrations of ONO-7579; PK model describing tumor concentrations of ONO-7579; PK/PD model describing a relationship between tumor concentrations of ONO-7579 and pTRKA levels in tumors; and PD/efficacy model describing a relationship between inhibition rate of pTRKA in tumors and tumor volume. Some data about plasma concentrations of ONO-7579 were obtained at several time points from individual mice, and plasma PK analyses were therefore performed using the ADVAN2 TRANS2 subroutines. Every data item about tumor concentrations of ONO-7579 and pTRKA levels in tumors was obtained from a single mouse, and analyses were performed using the ADVAN6 subroutines with tolerance set to nine by means of a naïve-pooled method, in which all data were fitted together as if they were obtained from a single individual. PD/efficacy modeling was performed using the ADVAN6 subroutines with tolerance set to nine by means of the first-order conditional estimation method with interaction. Interindividual variability in the parameters was assumed to

Downloaded from jpet.aspetjournals.org at ASPET Journals on April 20, 2024

JPET Fast Forward. Published on March 26, 2020 as DOI: 10.1124/jpet.119.264499
This article has not been copyedited and formatted. The final version may differ from this version.

follow the log-normal distribution. The residual error in all models was described by a proportional model. Model selection was guided by the minimum objective function value (OFV) for nested models. A decrease in OFV of >6.63 was considered statistically significant (P <0.01; one degree of freedom) for the addition of one parameter. Agreement between simulated and observed values was judged by visual predictive check, based on 1000 simulated replications of the study.

Plasma PK modeling. The data (n=1) for 0.06 mg/kg 24 h after the last dose were below the lower limit of quantification in the tumor growth study and were therefore excluded from the analysis. A one-compartment model with first-order absorption was used as a PK model:

$$\frac{dA_1}{dt} = -K_a \cdot A_1 \quad (1)$$

$$\frac{dA_2}{dt} = K_a \cdot A_1 - K_{el} \cdot A_2 \quad (2)$$

Where A_1 and A_2 are the ONO-7579 amounts in the depot and plasma compartments, respectively, K_a is the absorption rate constant, and K_{el} (clearance/distribution volume) is the elimination rate constant.

Tumor PK modeling. Tumor concentrations of ONO-7579 were described with a compartment model that would not influence pharmacokinetics in the central compartment.

$$\frac{dA_3}{dt} = K_{in} \cdot A_2 - K_{out} \cdot A_3 \quad (3)$$

Where A_3 is the ONO-7579 amount in the tumor compartment, K_{in} is the distribution rate constant, and K_{out} is the elimination rate constant.

Downloaded from jpet.aspetjournals.org at ASPET Journals on April 20, 2024

JPET Fast Forward. Published on March 26, 2020 as DOI: 10.1124/jpet.119.264499
This article has not been copyedited and formatted. The final version may differ from this version.

PK/PD modeling. pTRKA levels in the treatment group were expressed as the percent of control animal data. pTRKA was linked to tumor concentrations of ONO-7579 and described with the direct inhibitory E_{max} model. The equation is as follows:

$$R = 100 \cdot \left(1 - \frac{E_{maxR} \cdot {A_3}^{Hill_R}}{{EC_{50R}}^{Hill_R} + {A_3}^{Hill_R}}\right) \quad (4)$$

Where R is the pTRKA level in tumors. and E_{maxR}, EC_{50R}, and $Hill_R$ are drug-specific parameters representing the maximum inhibitory effect of pTRKA, the tumor ONO-7579 concentration that produces 50% of E_{maxR}, and Hill coefficient, respectively.

PD/efficacy modeling. The data for two mice in the control group, in which ulcers developed during the 12-day administration period, were excluded from the analysis. In the tumor growth model, a first-order tumor growth rate and a tumor death rate were assumed. Assuming that tumor growth would be suppressed according to the pTRKA inhibitory rate (100 − R), the effect was described with a sigmoid E_{max} model. The temporal tumor growth inhibitory effect until day 2 was also taken into account because a slight reduction in tumor volume was found at the first observation (day 2) after administration in all treatment groups, including the control group. Individual observed values at time 0 were used as initial values of tumor volume. The differential equations are as follows:

$$\frac{dT}{dt} = K_{tg} \cdot \left(1 - \frac{E_{maxT} \cdot (100 - R)^{Hill_T}}{{EC_{50T}}^{Hill_T} + (100 - R)^{Hill_T}}\right) \cdot T - K_{td} \cdot T \quad (5)$$

In case of time ≤day 2

$$\frac{dT}{dt} = K_{tg} \cdot \left(1 - \frac{E_{maxT} \cdot (100 - R)^{Hill_T}}{{EC_{50T}}^{Hill_T} + (100 - R)^{Hill_T}}\right) \cdot TEMP \cdot T - K_{td} \cdot T \quad (6)$$

Downloaded from jpet.aspetjournals.org at ASPET Journals on April 20, 2024

JPET Fast Forward. Published on March 26, 2020 as DOI: 10.1124/jpet.119.264499
This article has not been copyedited and formatted. The final version may differ from this version.

Where T is the tumor volume; K_{tg} and K_{td} are the first-order tumor growth and death rate constants, respectively; TEMP is the temporary tumor growth inhibition rate; and E_{maxT}, EC_{50T}, and $Hill_T$ are pTRKA-specific parameters representing the maximum inhibitory effect of K_{tg}, the pTRKA inhibition rate that produces 50% of E_{maxT}, and Hill coefficient, respectively.

Downloaded from jpet.aspetjournals.org at ASPET Journals on April 20, 2024

JPET Fast Forward. Published on March 26, 2020 as DOI: 10.1124/jpet.119.264499
This article has not been copyedited and formatted. The final version may differ from this version.

Results

Plasma PK modeling. Figure 3 shows observed and model-predicted plasma concentrations of ONO-7579 (represented by blue circles and lines), and Table 2 shows parameter estimates. Plasma concentrations of ONO-7579 reached the maximum 2 h after administration, and no accumulation due to repeated administration was observed. Exposure increased in a linear manner within the dose range considered. Results of the population PK analysis showed no interindividual variation incorporated in any parameter, or no difference observed in pharmacokinetics between the normal and xenograft mice.

Tumor PK modeling. Figure 3 shows observed and model-predicted tumor concentrations of ONO-7579 (represented by red triangles and lines), and Table 3 shows parameter estimates. The behavior of ONO-7579 was different regarding tumor and plasma concentrations. The tumor concentration reached the maximum 7 h after the single administration, and the trough tumor concentration after multiple administration was ≥10-fold higher than the plasma concentration.

PK/PD modeling. Figure 4 shows observed and model-predicted pTRKA levels after ONO-7579 administration. Depending on the dose of ONO-7579, pTRKA in tumors was inhibited. Observed pTRKA levels 2, 4, 7, 24, 38, and 48 h after the single administration of ONO-7579 0.6 mg/kg were 15.7, 7.0, 4.3, 16.7, 41.5, and 97.7%, respectively. The pTRKA levels recovered over time as ONO-7579 tumor concentration decreased. The observed pTRKA level was 7.8% at the trough concentration when ONO-7579 0.6 mg/kg was administered repeatedly, which suggested that pTRKA was almost completely inhibited at doses ≥0.6 mg/kg. Table 4 shows parameter estimates of the PK/PD model. Although two parameters, E_{maxR} and $Hill_R$, were

Downloaded from jpet.aspetjournals.org at ASPET Journals on April 20, 2024

JPET Fast Forward. Published on March 26, 2020 as DOI: 10.1124/jpet.119.264499
This article has not been copyedited and formatted. The final version may differ from this version.

estimated, no significant decrease in OFV was noted. Therefore, the two parameters were fixed at one. EC_{50R} was estimated to be 17.6 ng/g.

PD/efficacy modeling. Figure 5 shows observed and model-predicted tumor volume after multiple administration of ONO-7579, and Table 5 shows parameter estimates of the PD/efficacy model. ONO-7579 resulted in dose-dependent inhibition of tumor growth, and complete remission was observed with no bodyweight loss at 0.6 mg/kg (data not shown). EC_{50T} of the pTRKA inhibition rate for K_{tg} was estimated to be 91.3%, and $Hill_T$ was estimated to be 9.35. This means that a sharp increase in the antitumor effect of ONO-7579 occurs at a pTRKA inhibition rate near the EC_{50T}. Interindividual variation was incorporated in K_{td}, and interindividual variation of another parameter was additionally used, which was not significantly incorporated. The developed PD/efficacy model accurately reflected the observed values. Figure 6 shows the relationship between a pTRKA inhibition rate and a net tumor growth rate ($K_{tg} - K_{td}$), which were estimated with the PD/efficacy model. Ultimately, pTRKA inhibition rates ≥91.5% were required to reduce tumors.

Downloaded from jpet.aspetjournals.org at ASPET Journals on April 20, 2024

JPET Fast Forward. Published on March 26, 2020 as DOI: 10.1124/jpet.119.264499
This article has not been copyedited and formatted. The final version may differ from this version.

Discussion

ONO-7579 is an oral pan-TRK inhibitor that is expected to be highly effective and selective in inhibiting phosphorylation of all TRKs (Kawamoto et al., 2018). In this article, a relationship between pTRKA in tumors and antitumor effect in the murine KM12 xenograft model was defined using a PK/PD modeling approach to contribute to the selection of a recommended dose for clinical studies. There are two major approaches to apply PK/PD modeling to characterize *in vivo* exposure, biomarker response, and antitumor efficacy (Yamazaki et al., 2016). One is a two-step approach, where a PK/PD model and a PK/efficacy model are developed in parallel, followed by comparison of the PK/PD–PK/efficacy relationships. The other is an integrated modeling approach, where PK/PD/efficacy models are developed to simultaneously characterize the relationships of drug exposures to *in vivo* antitumor efficacy through biomarker responses. Both approaches are used to characterize molecularly targeted agents, and we considered that if a PD marker could be regarded as a single factor to control antitumor efficacy, the relationship between PD and efficacy would be clearly explained using an integrated modeling approach. The KM12 cell line is a colorectal cancer cell line harboring the *TPM3–NTRK1* fusion gene (Vaishnavi et al., 2013), and pTRKA initiates the activation of downstream intracellular signaling pathways (Deinhardt and Chao, 2014). In addition, larotrectinib, a first-generation pan-TRK inhibitor, inhibits KM12 cell proliferation and pTRKA at approximately the same concentrations as in *in vitro* studies (Pandre et al., 2018). Therefore, inhibition of tumor growth after ONO-7579 administration can be explained directly by changes in pTRKA; consequently, an integrated modeling approach was used.

Plasma ONO-7579 concentration was well described with an oral one-compartment model. Only data about plasma ONO-7579 concentrations in xenograft mice ≥2 h after administration

Downloaded from jpet.aspetjournals.org at ASPET Journals on April 20, 2024

JPET Fast Forward. Published on March 26, 2020 as DOI: 10.1124/jpet.119.264499
This article has not been copyedited and formatted. The final version may differ from this version.

were obtained, and the absorption rate constant could not be estimated without the data for normal mice. No differences in pharmacokinetics were found between normal and xenograft mice, and the model was considered to accurately describe absorption in xenograft mice. Tumor ONO-7579 concentrations were well described with an additional compartment, which did not influence plasma concentrations measurably. Although transfer parameters have no physiologic meaning, a description of the changes is required to consider pTRK behavior in the target. Tumor ONO-7579 concentrations were higher than plasma concentrations. It is the unbound fraction of a drug that normally penetrates into tissues: the more unbound drug in plasma, the more easily the drug penetrates into tissues. Our in-house data showed that plasma protein-binding of ONO-7579 in mice was 99.94%, which was extremely high; it was also shown that ONO-7579 was sufficiently distributed to tumor target tissue. One possible explanation is the enhanced permeability and retention effect. In solid cancers, high molecular weight compounds such as albumin-bound drugs leak preferentially into tumor tissue through permeable tumor vessels and are then retained in the tumor due to reduced lymphatic drainage (Matsumura and Maeda, 1986). Another possible explanation is the lysosomotropism of basic compounds. Lipophilic compounds with weak base properties readily diffuse across cell membranes, and when these drugs enter the acidic lumen of lysosomes, they become protonated and are trapped in the lysosomes (Goldman SD et al., 2009). ONO-7579 is also a weakly basic compound having an aminopyridine moiety in its structure and has high lipophilicity. Therefore, these mechanisms might have contributed to the accumulation of ONO-7579 in the tumor.

Although a delay in distribution from plasma to tumor was found, tumor concentrations and pTRKA levels were well described with a direct inhibitory E_{max} model. An indirect response model (Dayneka et al., 1993) was also considered, which did not perform better, and no temporal

Downloaded from jpet.aspetjournals.org at ASPET Journals on April 20, 2024

JPET Fast Forward. Published on March 26, 2020 as DOI: 10.1124/jpet.119.264499
This article has not been copyedited and formatted. The final version may differ from this version.

delay in inhibiting pTRKA was incorporated. Since phosphorylation of receptor tyrosine kinase is the first phase of signal transduction, it was considered reasonable to have a direct correlation with ONO-7579 concentration in the target tumor site.

There have been many reports about tumor growth models in xenograft mice (Mould et al., 2015), and tumor growth in the simplest model can be described with an exponential function. Tumor volume increased in a logarithmic manner over 12 days of ONO-7579 administration, and a model describing growth saturation (Kogame et al., 2013; Simeoni et al., 2004) was not used. In addition, a slight reduction in tumors was observed in all treatment groups, including the control group, at observation 2 days after ONO-7579 administration. A placebo effect is considered unlikely in the model animals. The cause of the temporary reduction in tumor volume was unknown; however, mice were only assigned to groups 3 days after tumor cells were grafted and ONO-7579 administration was started. The remaining graft cell suspension (0.1 mL) and/or inflammation at the injection site on grafting, might have biased the measurement of tumor volume 2 days after administration. In developing a PD/efficacy model, a significant reduction in the objective function (ΔOFV = −123.385) was noted when temporal effect up to day 2 was also incorporated into K_{tg}. Therefore, a model was developed with the temporal effect incorporated. Since predicted values in a final model accurately reflected observed values, the antitumor effect of ONO-7579 was considered properly evaluated.

The developed PD/efficacy model showed that ONO-7579 had a minimal antitumor effect at pTRKA inhibition rates ≤60%, but ONO-7579 started to sharply increase the antitumor effect at pTRKA inhibition rates >60%. These results indicate that there is a threshold pTRKA inhibition rate above which the antitumor effect is exerted. Interestingly, this “switch-like” behavior has also been reported in similar analyses conducted with other kinase inhibitors, such

Downloaded from jpet.aspetjournals.org at ASPET Journals on April 20, 2024

JPET Fast Forward. Published on March 26, 2020 as DOI: 10.1124/jpet.119.264499
This article has not been copyedited and formatted. The final version may differ from this version.

as: cobimetinib, a mitogen-activated protein/extracellular signal–regulated kinase kinase inhibitor studied in A375 xenografts (Wong et al., 2012); GDC-0879, a B-RAF kinase inhibitor studied in A375 xenografts (Wong et al., 2009); GDC-0834, a Bruton's tyrosine kinase inhibitor studied in a rat collagen-induced arthritis model (Liu et al., 2011); and vismodegib, a hedgehog-signaling pathway inhibitor studied in D5123 xenografts and medulloblastoma allografts (Wong et al., 2011).

Although the strategy for the development of novel kinase inhibitors appears to follow the historical maximum tolerated dose (MTD) based development, many drugs issued postmarketing requirements/postmarketing commitments by the United States Food and Drug Administration for dose optimization efforts due to safety concerns (Lu et al., 2016). PD biomarker monitoring in clinical development guides the optimized dose associated with biological activity. For example, ibrutinib and trametinib have been approved for non-MTD label doses by this strategy (Lu et al., 2016). Similarly, measuring pTRKA in tumors would allow us to propose a biologically effective dose lower than the MTD. From another point of view, considering that drug resistance has been found in TRK inhibitors in development (Drilon et al., 2016; Russo et al., 2016), a dosage where complete inhibition of pTRK is maintained throughout a dosing interval would be desirable to prevent the occurrence of drug resistance. Based on our results, a dosage required to fully (≥91.5%) and continuously inhibit pTRKA at the steady-state trough can be easily calculated and proposed for use in clinical studies of ONO-7579. In addition, the relationship between pTRKA inhibition and antitumor effect could be applied to other TRK inhibitors because their downstream signal is considered the same.

In conclusion, the PK/PD/efficacy models we developed in this study successfully identified a relationship between pTRKA inhibition and antitumor effect in a murine xenograft

Downloaded from jpet.aspetjournals.org at ASPET Journals on April 20, 2024

JPET Fast Forward. Published on March 26, 2020 as DOI: 10.1124/jpet.119.264499
This article has not been copyedited and formatted. The final version may differ from this version.

tumor model and demonstrated that pTRKA in tumors can be an effective biomarker to rationally design dosing regimens for early-stage clinical studies of ONO-7579.

Authorship Contributions

Participated in research design: Iida, Fujikawa, and Kozaki.

Conducted experiments: Fujikawa, Harada, and Hosokawa.

Performed data analysis: Iida.

Wrote or contributed to the writing of the manuscript: Iida, Ogawara, and Ohno.

Downloaded from jpet.aspetjournals.org at ASPET Journals on April 20, 2024

JPET Fast Forward. Published on March 26, 2020 as DOI: 10.1124/jpet.119.264499
This article has not been copyedited and formatted. The final version may differ from this version.

References

Dayneka NL, Garg V, and Jusko WJ (1993) Comparison of four basic models of indirect pharmacodynamic responses. J Pharmacokinet Biopharm 21: 457-478.

Deinhardt K, and Chao MV (2014) Trk receptors. Handb Exp Pharmacol 220: 103-119.

Doebele RC, Davis LE, Vaishnavi A, Le AT, Estrada-Bernal A, Keysar S, Jimeno A, Varella-Garcia M, Aisner DL, Li Y, Stephens PJ, Morosini D, Tuch BB, Fernandes M, Nanda N, and Low JA (2015) An oncogenic NTRK fusion in a patient with soft-tissue sarcoma with response to the tropomyosin-related kinase inhibitor LOXO-101. Cancer Discov 5: 1049-1057.

Drilon A, Laetsch TW, Kummar S, DuBois SG, Lassen UN, Demetri GD, Nathenson M, Doebele RC, Farago AF, Pappo AS, Turpin B, Dowlati A, Brose MS, Mascarenhas L, Federman N, Berlin J, El-Deiry WS, Baik C, Deeken J, Boni V, Nagasubramanian R, Taylor M, Rudzinski ER, Meric-Bernstam F, Sohal DPS, Ma PC, Raez LE, Hechtman JF, Benayed R, Ladanyi M, Tuch BB, Ebata K, Cruickshank S, Ku NC, Cox MC, Hawkins DS, Hong DS, and Hyman DM (2018) Efficacy of larotrectinib in TRK fusion-positive cancers in adults and children. N Engl J Med 378:731-739.

Drilon A, Li G, Dogan S, Gounder M, Shen R, Arcila M, Wang L, Hyman DM, Hechtman J, Wei G, Cam NR, Christiansen J, Luo D, Maneval EC, Bauer T, Patel M, Liu SV, Ou SH, Farago A, Shaw A, Shoemaker RF, Lim J, Hornby Z, Multani P, Ladanyi M, Berger M, Katabi N, Ghossein R, and Ho AL (2016) What hides behind the MASC: clinical response and acquired resistance to entrectinib after ETV6-NTRK3 identification in a mammary analogue secretory carcinoma (MASC). Ann Oncol 27: 920-926.

Downloaded from jpet.aspetjournals.org at ASPET Journals on April 20, 2024

JPET Fast Forward. Published on March 26, 2020 as DOI: 10.1124/jpet.119.264499
This article has not been copyedited and formatted. The final version may differ from this version.

Drilon A, Nagasubramanian R, Blake JF, Ku N, Tuch BB, Ebata K, Smith S, Lauriault V, Kolakowski GR, Brandhuber BJ, Larsen PD, Bouhana KS, Winski SL, Hamor R, Wu WI, Parker A, Morales TH, Sullivan FX, DeWolf WE, Wollenberg LA, Gordon PR, Douglas-Lindsay DN, Scaltriti M, Benayed R, Raj S, Hanusch B, Schram AM, Jonsson P, Berger MF, Hechtman JF, Taylor BS, Andrews S, Rothenberg SM, and Hyman DM (2017a) A next-generation TRK kinase inhibitor overcomes acquired resistance to prior TRK kinase inhibition in patients with TRK fusion-positive solid tumors. Cancer Discov 7: 963-972.

Drilon A, Siena S, Ou SI, Patel M, Ahn MJ, Lee J, Bauer TM, Farago AF, Wheler JJ, Liu SV, Doebele R, Giannetta L, Cerea G, Marrapese G, Schirru M, Amatu A, Bencardino K, Palmeri L, Sartore-Bianchi A, Vanzulli A, Cresta S, Damian S, Duca M, Ardini E, Li G, Christiansen J, Kowalski K, Johnson AD, Patel R, Luo D, Chow-Maneval E, Hornby Z, Multani PS, Shaw AT, and De Braud FG (2017b) Safety and antitumor activity of the multitargeted pan-TRK, ROS1, and ALK inhibitor entrectinib: combined results from two phase I trials (ALKA-372-001 and STARTRK-1). Cancer Discov 7: 400-409.

Friedman AA, Letai A, Fisher DE, and Flaherty KT (2015) Precision medicine for cancer with next-generation functional diagnostics. Nat Rev Cancer 15: 747-756.

Goldman SD, Funk RS, Rajewski RA, and Krise JP (2009) Mechanisms of amine accumulation in, and egress from, lysosomes. Bioanalysis 1:1445-59.

Kawamoto M, Ozono K, Oyama Y, Yamasaki A, Oda Y, and Onishi H (2018) The novel selective pan-TRK inhibitor ONO-7579 exhibits antitumor efficacy against human gallbladder cancer in vitro. Anticancer Res 38: 1979-1986.

Kogame A, Tagawa Y, Shibata S, Tojo H, Miyamoto M, Tohyama K, Kondo T, Prakash S, Shyu WC, and Asahi S (2013) Pharmacokinetic and pharmacodynamic modeling of hedgehog

Downloaded from jpet.aspetjournals.org at ASPET Journals on April 20, 2024

JPET Fast Forward. Published on March 26, 2020 as DOI: 10.1124/jpet.119.264499
This article has not been copyedited and formatted. The final version may differ from this version.

inhibitor TAK-441 for the inhibition of Gli1 messenger RNA expression and antitumor efficacy in xenografted tumor model mice. Drug Metab Dispos 41: 727-734.

Laetsch TW, DuBois SG, Mascarenhas L, Turpin B, Federman N, Albert CM, Nagasubramanian R, Davis JL, Rudzinski E, Feraco AM, Tuch BB, Ebata KT, Reynolds M, Smith S, Cruickshank S, Cox MC, Pappo AS, and Hawkins DS (2018) Larotrectinib for paediatric solid tumours harbouring NTRK gene fusions: phase 1 results from a multicentre, open-label, phase 1/2 study. Lancet Oncol 19: 705-714.

Lange AM, and Lo HW (2018) Inhibiting TRK proteins in clinical cancer therapy. Cancers 10: 105.

Liu L, Di Paolo J, Barbosa J, Rong H, Reif K, and Wong H (2011) Antiarthritis effect of a novel Bruton's tyrosine kinase (BTK) inhibitor in rat collagen-induced arthritis and mechanism-based pharmacokinetic/pharmacodynamic modeling: relationships between inhibition of BTK phosphorylation and efficacy. J Pharmacol Exp Ther 338: 154-163.

Lu D, Lu T, Stroh M, Graham RA, Agarwal P, Musib L, Li CC, Lum BL, and Joshi A (2016) A survey of new oncology drug approvals in the USA from 2010 to 2015: a focus on optimal dose and related postmarketing activities. Cancer Chemother Pharmacol 77: 459-76.

Matsumura Y, and Maeda H (1986) A new concept for macromolecular therapeutics in cancer chemotherapy: mechanism of tumoritropic accumulation of proteins and the antitumor agent smancs. Cancer Res 46: 6387-6392.

Mould DR, Walz AC, Lave T, Gibbs JP, and Frame B (2015) Developing exposure/response models for anticancer drug treatment: special considerations. CPT Pharmacometrics Syst Pharmacol 4: e00016.

Downloaded from jpet.aspetjournals.org at ASPET Journals on April 20, 2024

JPET Fast Forward. Published on March 26, 2020 as DOI: 10.1124/jpet.119.264499
This article has not been copyedited and formatted. The final version may differ from this version.

Pandre MK, Shaik S, Satya Pratap VVV, Yadlapalli P, Yanamandra M, and Mitra S (2018) A novel in-cell ELISA method for screening of compounds inhibiting TRKA phosphorylation, using KM12 cell line harboring TRKA rearrangement. Anal Biochem 545: 78-83.

Russo M, Misale S, Wei G, Siravegna G, Crisafulli G, Lazzari L, Corti G, Rospo G, Novara L, Mussolin B, Bartolini A, Cam N, Patel R, Yan S, Shoemaker R, Wild R, Di Nicolantonio F, Bianchi AS, Li G, Siena S, and Bardelli A (2016) Acquired resistance to the TRK inhibitor entrectinib in colorectal cancer. Cancer Discov 6: 36-44.

Sachs JR, Mayawala K, Gadamsetty S, Kang SP, and de Alwis DP (2016) Optimal dosing for targeted therapies in oncology: drug development cases leading by example. Clin Cancer Res 22: 1318-1324

Simeoni M, Magni P, Cammia C, De Nicolao G, Croci V, Pesenti E, Germani M, Poggesi I, and Rocchetti M (2004) Predictive pharmacokinetic-pharmacodynamic modeling of tumor growth kinetics in xenograft models after administration of anticancer agents. Cancer Res 64: 1094-1101.

Vaishnavi A, Capelletti M, Le AT, Kako S, Butaney M, Ercan D, Mahale S, Davies KD, Aisner DL, Pilling AB, Berge EM, Kim J, Sasaki H, Park S, Kryukov G, Garraway LA, Hammerman PS, Haas J, Andrews SW, Lipson D, Stephens PJ, Miller VA, Varella-Garcia M, Jänne PA, and Doebele RC (2013) Oncogenic and drug-sensitive NTRK1 rearrangements in lung cancer. Nat Med 19: 1469-1472.

Wang S, Zhou Q, and Gallo JM (2009) Demonstration of the equivalent pharmacokinetic/pharmacodynamic dosing strategy in a multiple-dose study of gefitinib. Mol Cancer Ther 8: 1438-1447.

Downloaded from jpet.aspetjournals.org at ASPET Journals on April 20, 2024

JPET Fast Forward. Published on March 26, 2020 as DOI: 10.1124/jpet.119.264499
This article has not been copyedited and formatted. The final version may differ from this version.

Wong H, Alicke B, West KA, Pacheco P, La H, Januario T, Yauch RL, de Sauvage FJ, and Gould SE (2011) Pharmacokinetic-pharmacodynamic analysis of vismodegib in preclinical models of mutational and ligand-dependent Hedgehog pathway activation. Clin Cancer Res 17: 4682-4692.

Wong H, Belvin M, Herter S, Hoeflich KP, Murray LJ, Wong L, and Choo EF (2009) Pharmacodynamics of 2-[4-[(1E)-1-(hydroxyimino)-2,3-dihydro-1H-inden-5-yl]-3-(pyridine-4-yl)-1H-pyrazol-1-yl]ethan-1-ol (GDC-0879), a potent and selective B-Raf kinase inhibitor: understanding relationships between systemic concentrations, phosphorylated mitogen-activated protein kinase kinase 1 inhibition, and efficacy. J Pharmacol Exp Ther 329: 360-367.

Wong H, Bohnert T, Damian-Iordache V, Gibson C, Hsu CP, Krishnatry AS, Liederer BM, Lin J, Lu Q, Mettetal JT, Mudra DR, Nijsen MJMA, Schroeder P, Schuck E, Suryawanshi S, Trapa P, Tsai A, Wang H, and Wu F (2017) Translational pharmacokinetic-pharmacodynamic analysis in the pharmaceutical industry: an IQ Consortium PK-PD Discussion Group perspective. Drug Discov Today 22: 1447-1459.

Wong H, Vernillet L, Peterson A, Ware JA, Lee L, Martini JF, Yu P, Li C, Del Rosario G, Choo EF, Hoeflich KP, Shi Y, Aftab BT, Aoyama R, Lam ST, Belvin M, and Prescott J (2012) Bridging the gap between preclinical and clinical studies using pharmacokinetic-pharmacodynamic modeling: an analysis of GDC-0973, a MEK inhibitor. Clin Cancer Res 18: 3090-3099.

Yamazaki S (2013) Translational pharmacokinetic-pharmacodynamic modeling from nonclinical to clinical development: a case study of anticancer drug, crizotinib. AAPS J 15: 354-366.

Downloaded from jpet.aspetjournals.org at ASPET Journals on April 20, 2024

JPET Fast Forward. Published on March 26, 2020 as DOI: 10.1124/jpet.119.264499
This article has not been copyedited and formatted. The final version may differ from this version.

Yamazaki S, Lam JL, Zou HY, Wang H, Smeal T, and Vicini P (2015) Mechanistic understanding of translational pharmacokinetic-pharmacodynamic relationships in nonclinical tumor models: a case study of orally available novel inhibitors of anaplastic lymphoma kinase. Drug Metab Dispos 43: 54-62.

Yamazaki S, Spilker ME, and Vicini P (2016) Translational modeling and simulation approaches for molecularly targeted small molecule anticancer agents from bench to bedside. Expert Opin Drug Metab Toxicol 12: 253-265

Downloaded from jpet.aspetjournals.org at ASPET Journals on April 20, 2024

JPET Fast Forward. Published on March 26, 2020 as DOI: 10.1124/jpet.119.264499
This article has not been copyedited and formatted. The final version may differ from this version.

Footnotes

This work was funded by Ono Pharmaceutical Company Limited.

Downloaded from jpet.aspetjournals.org at ASPET Journals on April 20, 2024

JPET Fast Forward. Published on March 26, 2020 as DOI: 10.1124/jpet.119.264499
This article has not been copyedited and formatted. The final version may differ from this version.

Figure Legends

Figure 1. Structural formula of ONO-7579.

Figure 2. Graphical abstract of PK/PD/efficacy models. Plasma concentrations (C_p) of ONO-7579 were described with an oral one-compartment model where a drug is transferred from a depot compartment at the absorption rate constant (K_a) and eliminated at the elimination rate constant (K_{el}). Assuming that concentrations of ONO-7579 in tumors (C_t), which are sites of ONO-7579 action, would be transferred from the central compartment and eliminated at the distribution rate constants of K_{in} and K_{out}, C_t was described with an additional compartment that would not influence pharmacokinetics in the central compartment. pTRKA, an effective biomarker, was assumed to be linked to C_t and inhibited according to the E_{max} model. The changes in tumor volume were described with the first-order tumor growth rate constant (K_{tg}) and the tumor death rate constant (K_{td}). K_{tg} was assumed to be inhibited, according to the E_{max} model, as pTRKA was inhibited.

Figure 3. Observed and model-predicted plasma and tumor concentrations of ONO-7579 after single administration of ONO-7579 in normal mice (A), in KM12 xenograft mice (B), or after multiple administration of ONO-7579 in KM12 xenograft mice (C). Circles represent observed plasma concentrations, blue lines represent median predicted plasma concentrations, and blue areas are 90% prediction intervals of predicted plasma concentrations. Triangles represent observed tumor concentrations, red lines represent median predicted tumor concentrations, and red areas are 90% prediction intervals of predicted tumor concentrations.

Downloaded from jpet.aspetjournals.org at ASPET Journals on April 20, 2024

JPET Fast Forward. Published on March 26, 2020 as DOI: 10.1124/jpet.119.264499
This article has not been copyedited and formatted. The final version may differ from this version.

Figure 4. Observed and model-predicted pTRKA levels after single (A) or multiple (B) administration of ONO-7579 in KM12 xenograft mice. Concentration-response relationship between pTRKA and tumor concentrations of ONO-7579 (C). Symbols represent observed pTRKA levels, lines represent median predicted pTRKA levels, and areas are 90% prediction intervals.

Figure 5. Observed and model-predicted tumor volumes after multiple administration of ONO-7579 in KM12 xenograft mice. Symbols represent observed tumor volume, solid lines represent median predicted tumor volume, and areas are 90% prediction intervals.

Figure 6. Simulated net tumor growth rate and pTRKA inhibition. Dashed lines represent an apparent tumor growth rate of 0.

Downloaded from jpet.aspetjournals.org at ASPET Journals on April 20, 2024

JPET Fast Forward. Published on March 26, 2020 as DOI: 10.1124/jpet.119.264499
This article has not been copyedited and formatted. The final version may differ from this version.

Tables

Table 1. Antibodies used to measure phosphorylated TRKA and total TRKA with electrochemiluminescence

	Phospho-TRK detection plate	**Total-TRK detection plate**
Capture antibody	Mouse anti-TRK antibody (Santa Cruz Biotechnology)	Rabbit anti-TRK antibody (Cell Signaling)
Detect antibody	Rabbit anti-phospho-TRK antibody (Cell Signaling)	Mouse anti-TRK antibody (Santa Cruz Biotechnology)
Secondary antibody	SULFO-TAG labeled anti-rabbit antibody (Goat) (Meso scale discovery)	SULFO-TAG labeled anti-mouse antibody (Goat) (Meso scale discovery)

Downloaded from jpet.aspetjournals.org at ASPET Journals on April 20, 2024

JPET Fast Forward. Published on March 26, 2020 as DOI: 10.1124/jpet.119.264499
This article has not been copyedited and formatted. The final version may differ from this version.

Table 2. PK parameter estimates of plasma ONO-7579 after oral administration of ONO-7579 in KM12 xenograft or normal mice

Parameters (units)	**Definition**	**Estimates (RSE%)**
K_a (h^{-1})	Absorption rate constant	0.991 (19.5)
CL/F (L/h/kg)	Oral clearance	0.426 (4.8)
V/F (L/kg)	Oral volume of distribution	2.93 (5.9)
ε prop (%)	Proportional residual error	45.5 (12.9)

RSE%, relative standard error computed as the ratio between the standard error and the parameter estimate, multiplied by 100.

Downloaded from jpet.aspetjournals.org at ASPET Journals on April 20, 2024

JPET Fast Forward. Published on March 26, 2020 as DOI: 10.1124/jpet.119.264499
This article has not been copyedited and formatted. The final version may differ from this version.

Table 3. PK parameter estimates of tumor ONO-7579 after oral administration of ONO-7579 in KM12 xenograft mice

Parameters (units)	**Definition**	**Estimates (RSE%)**
K_{in} (h^{-1})	Distribution rate constant	0.228 (7.9)
K_{out} (h^{-1})	Elimination rate constant	0.156 (5.7)
ε prop (%)	Proportional residual error	43.0 (15.9)

RSE%, relative standard error computed as the ratio between the standard error and the parameter estimate, multiplied by 100.

Downloaded from jpet.aspetjournals.org at ASPET Journals on April 20, 2024

JPET Fast Forward. Published on March 26, 2020 as DOI: 10.1124/jpet.119.264499
This article has not been copyedited and formatted. The final version may differ from this version.

Table 4. PD parameter estimates of ONO-7579 for pTRKA after oral administration of ONO-7579 in KM12 xenograft mice

Parameters (units)	**Definition**	**Estimates (RSE%)**
E_{maxR}	Maximum inhibitory effect of pTRKA	1 FIX
EC_{50R} (ng/g)	Drug concentration causing 50% of E_{maxR}	17.6 (6.5)
$Hill_R$	Hill coefficient	1 FIX
ε prop (%)	Proportional residual error	33.8 (14.2)

RSE%, relative standard error computed as the ratio between the S.E. and the parameter estimate multiplied by 100.

Downloaded from jpet.aspetjournals.org at ASPET Journals on April 20, 2024

JPET Fast Forward. Published on March 26, 2020 as DOI: 10.1124/jpet.119.264499
This article has not been copyedited and formatted. The final version may differ from this version.

Table 5. PD parameter estimates of ONO-7579 for tumor growth after oral administration of ONO-7579 in KM12 xenograft mice

Parameters (units)	**Definition**	**Estimates (RSE%)**
E_{maxT}	Maximum inhibitory effect of K_{tg}	1 FIX
EC_{50T} (%)	pTRKA inhibition rate causing 50% of E_{maxT}	91.3 (3.6)
$Hill_T$	Hill coefficient	9.35 (27.7)
K_{tg} (h^{-1})	Tumor growth rate constant	0.0198 (15.7)
K_{td} (h^{-1})	Tumor death rate constant	0.00983 (30.0)
TEMP	Temporary tumor growth inhibition rate	0.272 (49.6)
ω K_{td} (%)	Interindividual variability on K_{td}	12.3 (77.5)
ε prop (%)	Proportional residual error	15.3 (19.4)

RSE%, relative standard error computed as the ratio between the standard error and the parameter estimate, multiplied by 100.

Downloaded from jpet.aspetjournals.org at ASPET Journals on April 20, 2024

JPET Fast Forward. Published on March 26, 2020 as DOI: 10.1124/jpet.119.264499
This article has not been copyedited and formatted. The final version may differ from this version.

Figures

Figure 1

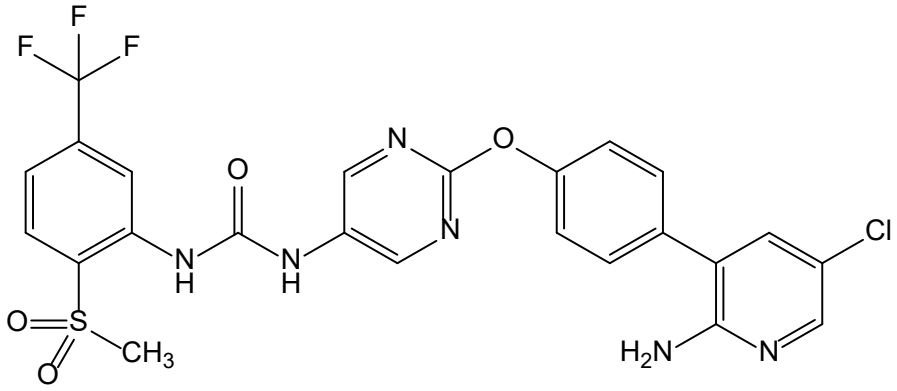

Downloaded from jpet.aspetjournals.org at ASPET Journals on April 20, 2024

JPET Fast Forward. Published on March 26, 2020 as DOI: 10.1124/jpet.119.264499
This article has not been copyedited and formatted. The final version may differ from this version.

Figure 2

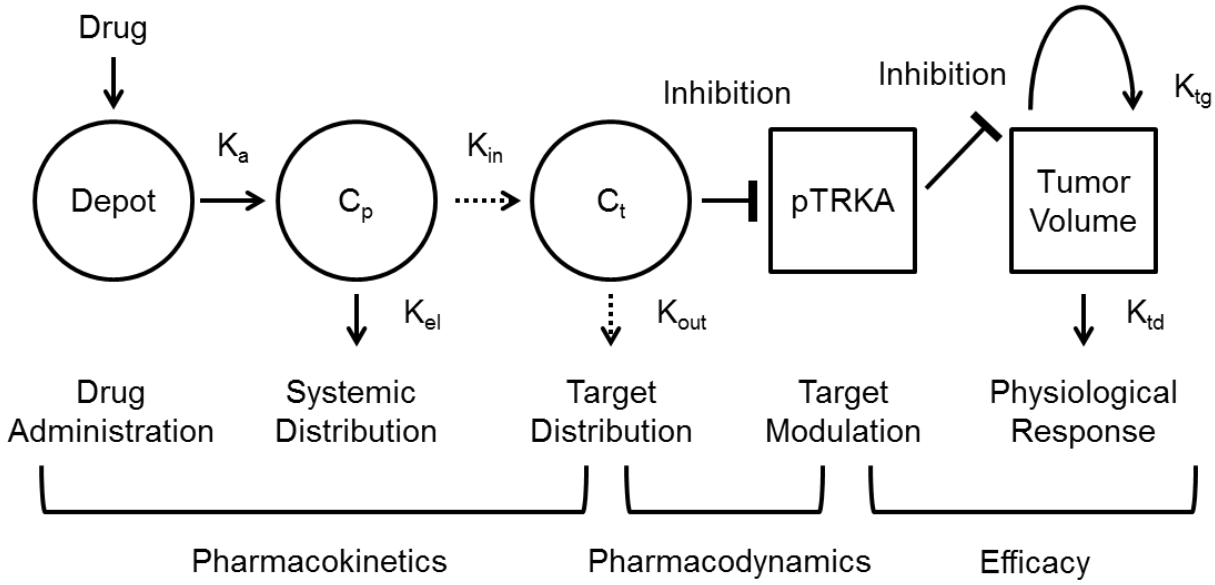

Downloaded from jpet.aspetjournals.org at ASPET Journals on April 20, 2024

JPET Fast Forward. Published on March 26, 2020 as DOI: 10.1124/jpet.119.264499
This article has not been copyedited and formatted. The final version may differ from this version.

Figure 3

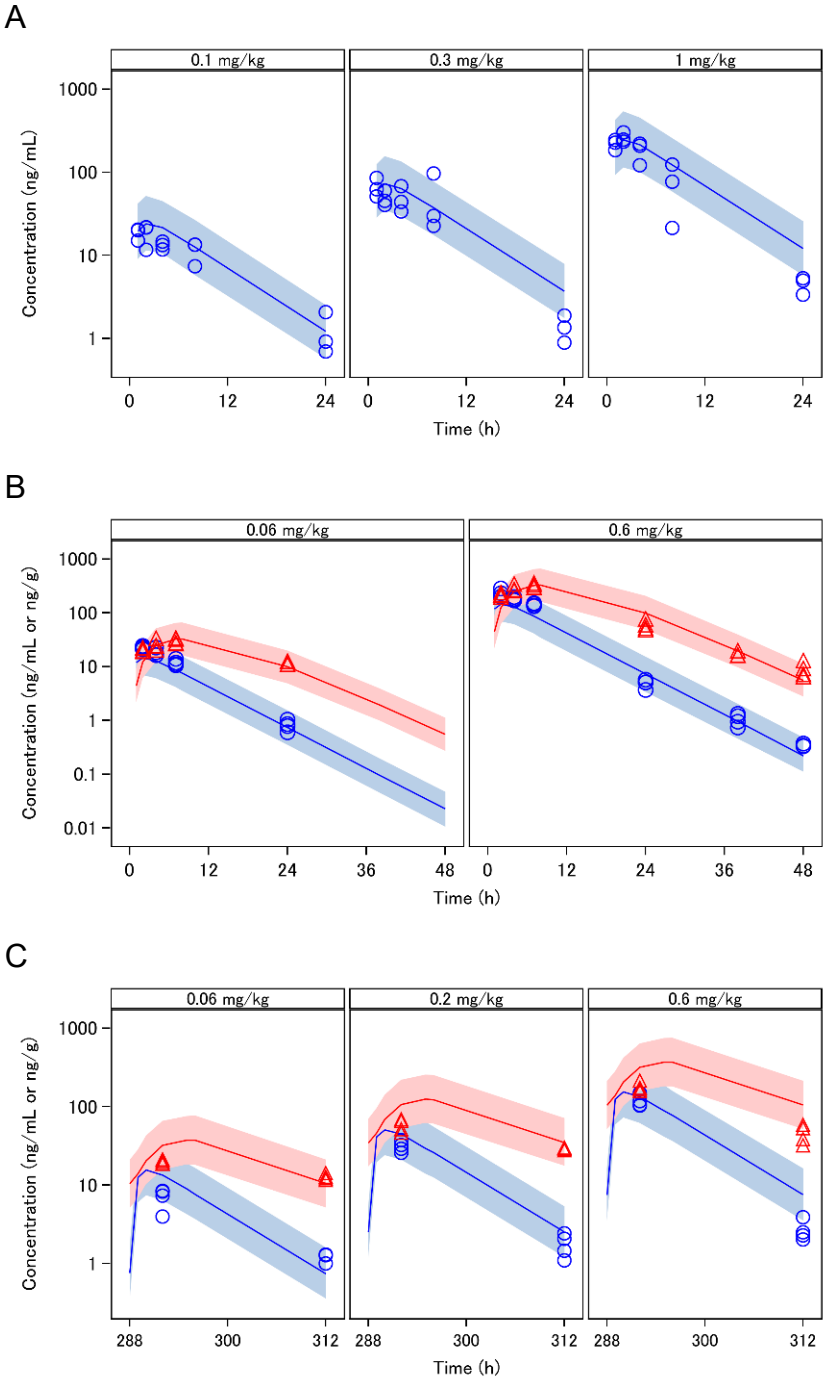

Downloaded from jpet.aspetjournals.org at ASPET Journals on April 20, 2024

JPET Fast Forward. Published on March 26, 2020 as DOI: 10.1124/jpet.119.264499
This article has not been copyedited and formatted. The final version may differ from this version.

Figure 4

A

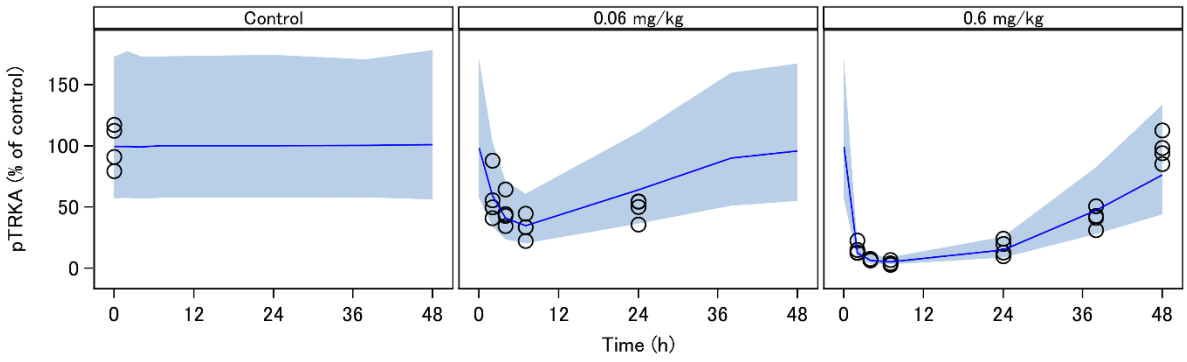

B

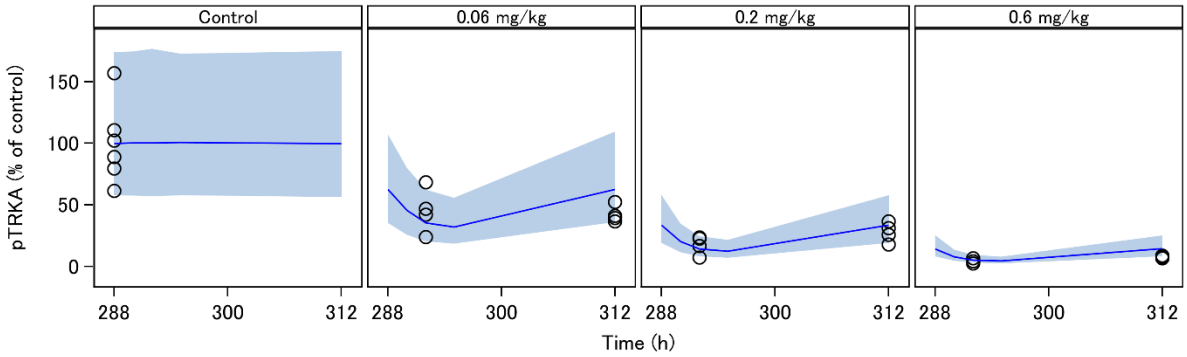

C

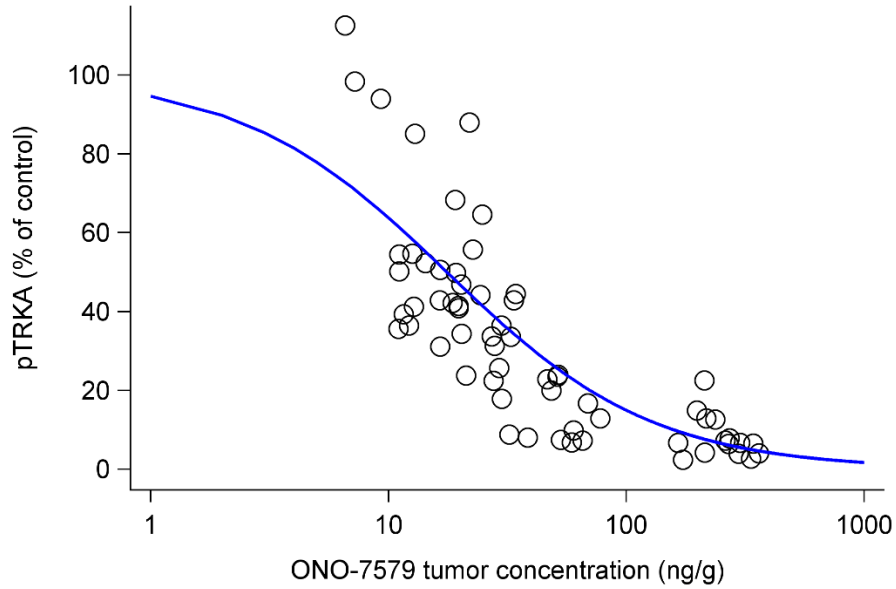

Downloaded from jpet.aspetjournals.org at ASPET Journals on April 20, 2024

JPET Fast Forward. Published on March 26, 2020 as DOI: 10.1124/jpet.119.264499
This article has not been copyedited and formatted. The final version may differ from this version.

Figure 5

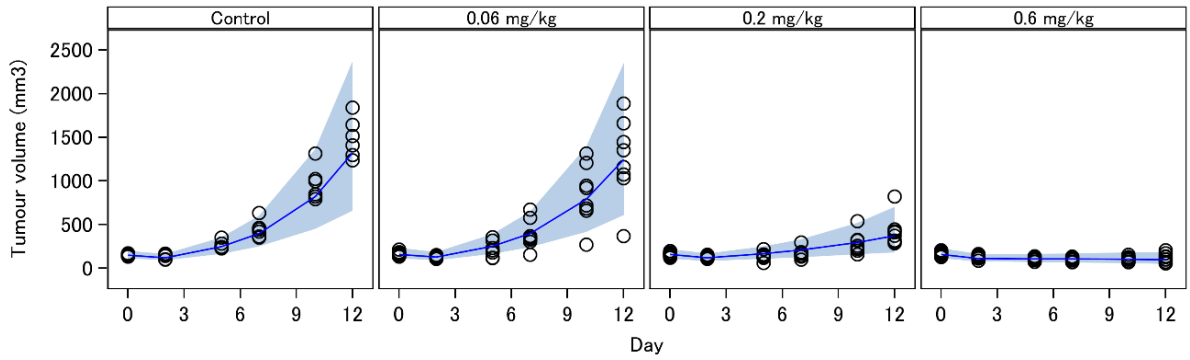

Downloaded from jpet.aspetjournals.org at ASPET Journals on April 20, 2024

JPET Fast Forward. Published on March 26, 2020 as DOI: 10.1124/jpet.119.264499
This article has not been copyedited and formatted. The final version may differ from this version.

Figure 6

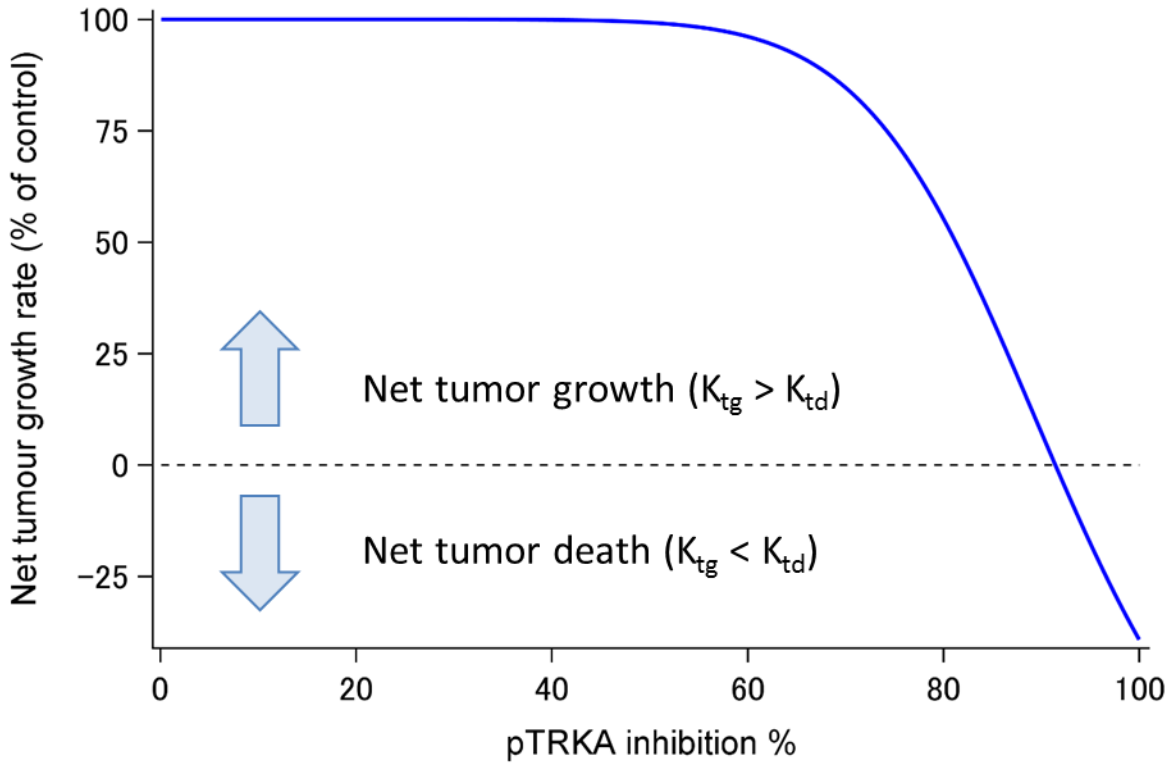

Downloaded from jpet.aspetjournals.org at ASPET Journals on April 20, 2024